

BITLIS EREN ÜNIVERSITESI FEN BİLİMLERİ DERGİSİ



ISSN: 2147-3129 / e-ISSN: 2147-3188

Article Type: Research Article Received : April 29, 2025 Revised : June 19, 2025 Accepted : July 8, 2025

DOI : 10.17798/bitlisfen.1687018

:2025 Year Volume :14 :3 Issue **Pages** :1610-1624



PHOTOCATALYTIC PROPERTIES OF CHITOSAN-COATED PESA SPHERES CONTAINING GALLIUM(III) NITRATE: SYNTHESIS AND CHARACTERIZATION

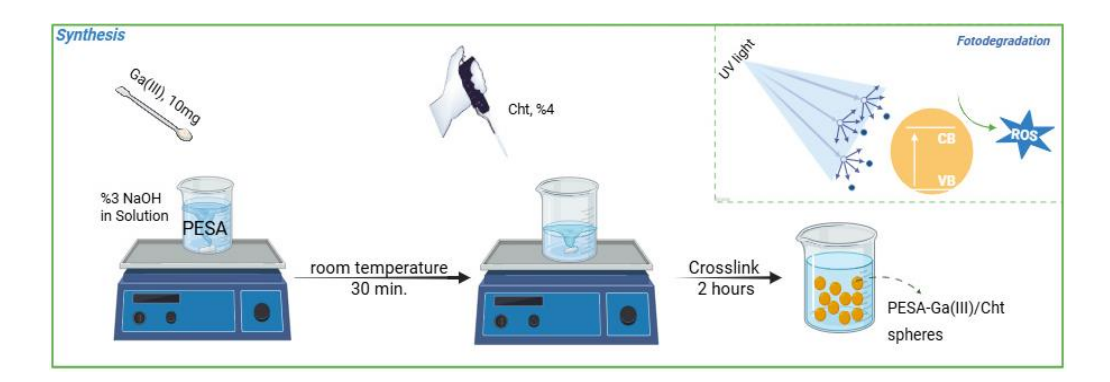
Deniz DOĞAN 1 D

¹ Kırıkkale University, Chemistry Department, Kırıkkale, Türkiye, <u>denizdogan@kku.edu.tr</u>

ABSTRACT

In this study, the photocatalytic effect of Chitosan (Cht) -Coated polyanetholsulfonic acid (PESA) Spheres Containing Gallium(III) Nitrate (Ga(NO₃)₃) on methylene blue (MB), a cationic dye, was investigated. The spheres were synthesized by dropwise addition of a chitosan solution to a PESA-Ga(III) solution prepared in a sodium hydroxide (NaOH) solution. It is known that the morphological properties of spheres change in the presence of metal. For this purpose, the surface morphology was determined by Scanning Electron Microscopy (SEM). Functional group analysis was determined using Fourier Transform Infrared (FTIR) Spectrometry. The concentration of Gallium ions remaining in the solution at the end of the reaction was determined by Inductively Coupled Plasma Optical Emission Spectroscopy (ICP-OES) analysis. A UV-C tube lamp was used to photocatalytically degrade the methylene blue dye. The dye degradation changes were then analyzed in a UV-VIS spectrophotometer. Furthermore, Tauc's formula determined the band gaps with the help of Chitosan-Coated PESA Spheres Containing Ga(NO₃)₃ (PESA- Ga(III)/Cht) and Chitosan-Coated PESA Spheres (PESA/Cht) UV spectra. It was observed that the photocatalytic effect increased with the incorporation of Ga(NO₃)₃ into the polymer structure.

Photocatalytic effect, Methylene blue, Gallium(III) Nitrate, Chitosan, PESA, **Keywords:** Dye degradation.



1 INTRODUCTION

Recently, excessive pollution of water resources with organic pollutants is increasingly endangering all life forms [1], [2]. Among these pollutants, cationic dyes such as methylene blue (MB) [3], which pose a significant environmental threat today, are highly harmful to living ecosystems due to their water solubility and toxicity. MB is frequently used in both medical and industrial fields [4], [5]. MB, which is used in staining to enhance the visibility of cells and microorganisms under the microscope, is also employed as an antiseptic in superficial injuries [5], [6], [7]. MB, a synthetic aniline dye, is used as a colored substance in the textile industry [8]. After this use, significant pollution of dyestuffs occurs in the water. Therefore, the degradation of MB is of great importance for protecting clean water resources [9], [10].

Photocatalytic treatment technologies are emerging, especially with metal-based catalysts that can operate under UV light [11]. Photocatalysts used for this purpose are very advantageous in terms of being environmentally friendly and reusable. Photocatalytic systems are activated using UV light energy and effectively degrade toxic substances such as cyanide, phosphorus, and difficult-to-degrade aromatic compounds through the electron-hole pairs they produce [11], [12], [13]. These systems not only minimize secondary pollution but also allow for rapid degradation through advanced oxidation processes (AOPS), which have gained wide acceptance in industrial wastewater treatment.

Chitosan, which can be classified as a natural catalyst, is used as a biodegradable, cheap, and multifunctional biopolymer as a support material for photocatalyst structures [14], [15], [16]. Thanks to its amino and hydroxyl groups, it can easily form complexes with metal ions [15], [17]. Its ability to act as a ligand for transition and post-transition metals makes it a suitable candidate for developing hybrid functional materials.

However, the photocatalytic effect of polymers containing sulfone groups such as polyanetholsulfonic acid (PESA) is quite limited in the literature. Since the ability of polymers containing sulfone groups to form complexes with metal ions is quite good [18], it further increases the photocatalytic activity. PESA, a polyelectrolyte with strong anionic character, can enhance metal ion dispersion and stabilization within the polymer matrix, thereby contribute to increased active surface area and electron transfer efficiency.

Gallium(III) is a metal ion that has attracted interest in photocatalytic applications in recent years. Thanks to its electron structure properties and oxidative stability, it can form active sites and increase catalytic activity. In addition, gallium-based catalysts have been reported to

exhibit high photocatalytic efficiency due to their ability to participate in multielectron redox reactions, low toxicity, and stable oxidation states [19], [20]. However, the literature on photocatalytic studies with biopolymer-supported Ga(III) systems is limited.

Rocha et al. reported 60% photodegradation of methylene blue using Gallium(III) reinforced hydroxyapatite particles [19]. In another study, Kujur et al. investigated the photocatalytic degradation of Rhodamine B dye using magnetic GaFeO₃ nanoparticles synthesized with gallium ions and reported a 68% removal rate [21]. Messemeche et al. reported a 94% photodegradation of methylene blue using gallium-doped TiO₂ thin films [22]. Parveen et al. reported 72% photodegradation of Rhodamine B dye in their study using Ga(III) [23]. This represents a promising opportunity to explore Ga(III)-based hybrid photocatalysts in combination with biopolymers and functional polymers such as PESA for synergistic effects.

In this study, Chitosan-Coated PESA Spheres Containing Ga(NO₃)₃ were synthesized, and their photocatalytic activity on the degradation of methylene blue under UV light was investigated. Various analytical methods characterized the spheres structural, morphological, and optical properties, and their photocatalytic degradation kinetics were evaluated using pseudo-first-order and pseudo-second-order kinetic models. This study aims to develop a low-cost photocatalyst to remove MB dyestuff in an easy and sustainable way. This novel material combines the chemical interaction capacity of PESA, the biocompatibility and functional group abundance of chitosan, and the catalytic potential of Ga(III), representing a multifunctional approach to organic pollutant remediation.

2 MATERIAL AND METHOD

Chitosan (medium molecular weight), Polyanetholsulfonic acid, Gallium (III) Nitrate Hydrate (99.99%), and Methylene blue (82%) were obtained from Aldrich. Sodium Hydroxide (99%) was obtained from Merck. Other chemicals used were of analytical purity and purchased from Merck.

2.1 Synthesis of Chitosan-Coated PESA Spheres Containing Gallium(III) Nitrate Spheres

Chitosan-coated polyanetholsulfonic acid spheres containing gallium (III) nitrate were synthesized in 3 steps. In the first step, a 0.2% by-volume solution of PESA was prepared in NaOH solution (3%, 50 mL). Then, 10 mg of Ga(NO₃)₃ was added. It was stirred for 30 minutes until the metal salt dissolved. In the second step, chitosan solution (v/v 4%) in 1% acetic acid

solution was prepared in another beaker. In the last step, the chitosan solution was added dropwise to the PESA-Ga(NO₃)₃ dissolved in NaOH solution to obtain a sphere. PESA-Ga(III)/Cht spheres were obtained by cross-linking with the help of NaOH. After 2 hours, the spheres were washed 3 times with distilled water and dried in an oven at 40 °C.

2.2 Characterization

After the synthesis of PESA- Ga(III)/Cht, the concentration of gallium(III) ions from the solution remaining at the end of the reaction was determined by ICP-OES (Spectroblue/FMS36, Germany). Scanning Electron Microscopy (SEM, JEOL, 5600) was used to determine the surface morphology of the spheres. Functional group analysis was determined using a Fourier Transform Infrared (FTIR) Spectrometer (Bruker Vertex 70V). The optical properties of the spheres and changes in dye concentrations were analyzed using a UV-VIS spectrophotometer (Shimadzu, Model 1280).

2.3 Photocatalytic Effect

UV-C tube lamp (lamp specifications; 15 W, Philips Netherlands G15T8) was used to determine the photocatalytic effect of the synthesized spheres on methylene blue.

Firstly, 10 ppm MB was prepared in pure water. Different amounts (25, 50, 100, and 150 mg) of spheres were added to the prepared dye solution and stirred in the dark for 15 min. After reaching equilibrium, they were exposed to UV light for 240 min. At the end of the time, the absorbance value at 664 nm, which is known to be the maximum wavelength of the dye, was determined in a UV-VIS spectrophotometer. The process was repeated using different concentrations (10-25-50-100 ppm) of dye solution with the determined optimum amount of spheres. Then, under the same conditions, the optimum amount of spheres and dye concentration, time study, and reusability of the spheres were investigated. The results were determined by calculating the amount of dye remaining in the solution according to Equation 1 [24]. (A₀ an A_t, the initial absorption and absorption at time t, respectively.)

$$Removal = \frac{A_0 - A_t}{A_0} \times 100 \tag{1}$$

3 RESULTS AND DISCUSSION

PESA-Ga(III)/Cht spheres were obtained by dropwise addition of chitosan to PESA-Ga(NO₃)₃ solution dissolved in NaOH solution. The structure of the spheres was determined by ICP-OES, SEM, and FTIR analysis. The photocatalytic effect of the spheres on the dye was determined by UV-VIS analysis.

Firstly, the amount of Ga(III) ions from the solution remaining at the end of the reaction was determined by ICP-OES analysis. Accordingly, it was determined that it contained 8.7mg Ga(III) per 1g sphere.

3.1 SEM Analysis

SEM images of PESA/Cht and PESA-Ga(III)/Cht spheres at different magnifications are shown in Figure 1. Accordingly, it is observed that the spheres generally have a smooth spherical shape. The measurements made with the FIJI program determined that the spheres had an average size of 1.014±0.03 mm.

The SEM images presented in this study provide crucial insights into the surface characteristics of the synthesized PESA-Ga(III)/Cht composite spheres. Morphological properties play a critical role in the photocatalytic performance of polymer–metal hybrid systems, as they directly influence the active surface area, light absorption, and dye adsorption–desorption dynamics.

The observed SEM micrographs exhibit spherical and relatively uniform particle morphologies, with evident surface roughness and porosity, particularly in the Ga(III)-incorporated structures.

It is known that the morphological properties of the spheres change in the presence of a metal [5]. Figure 1 shows that the surface is homogeneous and non-porous with the introduction of Ga(III) into the structure. It is also seen that in the presence of Ga(III), it reaches a more uniform sphere form. This topography is significant, as it facilitates enhanced interaction between the dye molecules and the photocatalyst. Moreover, such a morphology supports improved UV light penetration and scattering, which is essential for the efficient generation of electron—hole pairs in UV-activated systems[25], [26]. For rough surfaces, this system can be explained as follows. On rough surfaces, UV rays interact with a large number of microsurfaces, resulting in multiple scattering that can reduce penetration. A smooth chitosan sphere, on the

other hand, can reduce scattering, allowing light to reach its target more directly and penetrate deeper.

Importantly, the spherical shape of the particles supports isotropic diffusion of reactants and photons around the catalyst, allowing for more uniform photocatalytic degradation. The microscale roughness likely arises from the coordinated incorporation of Ga(III) ions into the polymeric matrix, which not only stabilizes the morphology but also induces surface heterogeneity—a factor known to enhance light-trapping and local electric field enhancement, both of which are crucial for boosting photocatalytic efficiency [27], [28].

In the context of photovoltaic or more precisely, photocatalytic effects, the presence of Ga(III) is expected to serve as a charge trapping and transfer mediator, improving the separation of photo-generated electron—hole pairs. The SEM-supported morphology suggests that the Ga(III) ions are well-dispersed within the chitosan-PESA network, avoiding agglomeration, and thereby maximizing the available surface for catalysis [29], [30], [31], [32].

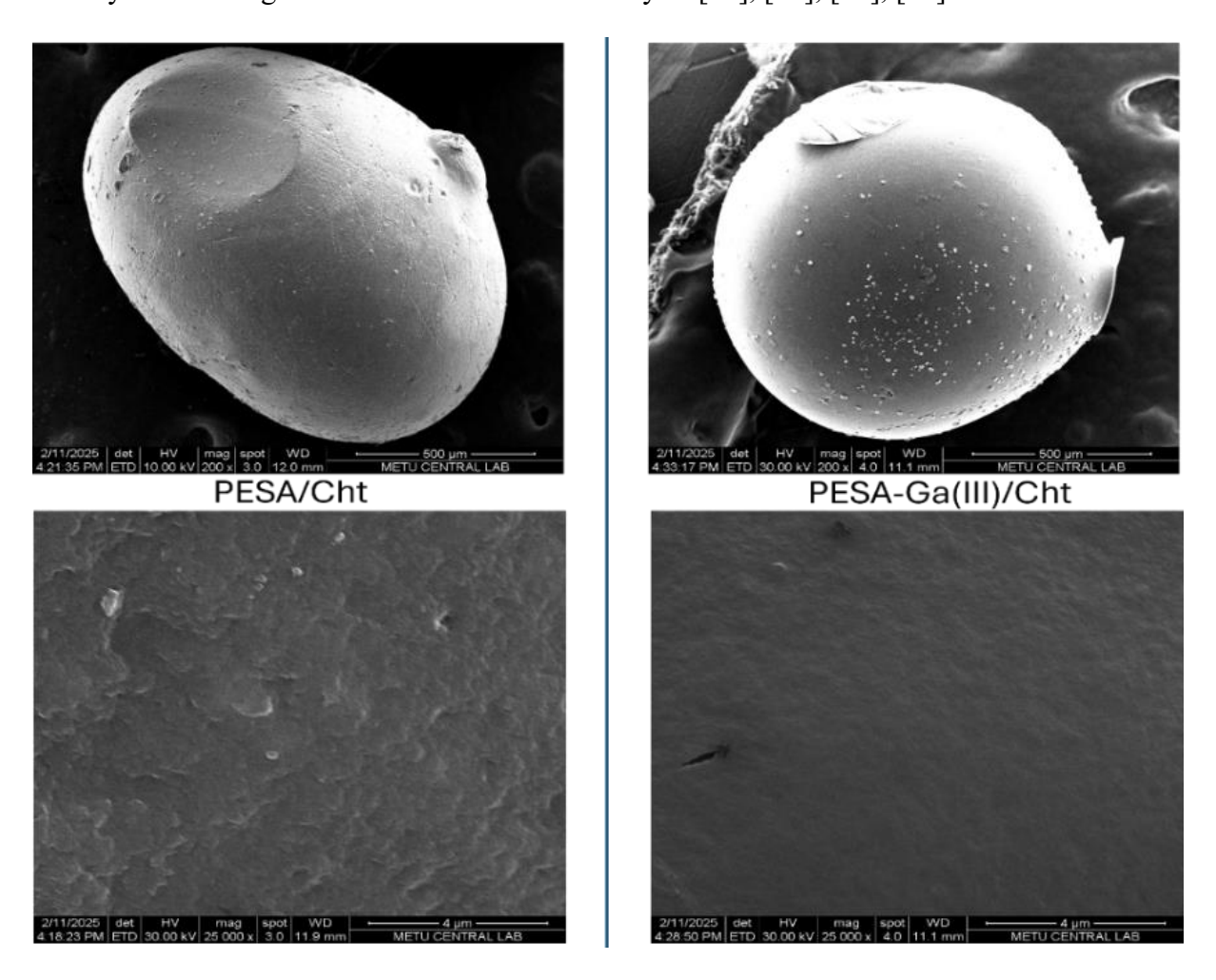


Figure 1. SEM images of PESA/Cht and PESA-Ga(III)/Cht spheres

Additionally, chitosan coating appears to contribute to a more structured and interconnected surface, potentially acting as a functional interface that enhances the electron transport pathway. This is particularly relevant in Ga(III)-based systems, where efficient charge separation and transfer is often a limiting step in the photocatalytic cycle [33].

From a materials design standpoint, the SEM evidence strongly supports the suitability of the synthesized spheres for UV-driven dye degradation applications. The combination of morphological features—namely sphericity, roughness, and hierarchical texture—aligns well with the study's goal of developing an efficient hybrid photocatalyst for methylene blue removal [34].

The SEM analyses validate the successful formation of Ga(III)-incorporated chitosancoated PESA spheres with favorable morphological attributes for photocatalytic applications. These structures are likely to provide enhanced dye adsorption capacity, efficient light harvesting, and improved charge carrier dynamics—all of which are key parameters for highperformance photocatalysts. The observed morphology is therefore not only consistent with the intended synthesis strategy but also instrumental in achieving the functional objectives of the study [26], [35].

3.2 FTIR Analysis

FTIR analysis was performed to determine the characteristic functional groups present in the structure of PESA/Cht and PESA-Ga(III)/Cht spheres. FTIR spectra of PESA/Cht and PESA-Ga(III)/Cht spheres are given in Figure 2. For PESA/Cht spheres: In the spectrum, vibration bands specific to PESA polymer and Cht (Chitosan) polysaccharide, for PESA-Ga(III)/Cht spheres: In addition to the PESA/Cht spectrum, new bands or shifts in existing bands related to the interaction of Ga(III) ions with chitosan and PESA were tried to be observed.

The region at 3373 cm⁻¹ corresponds to the stretching vibrations of -OH and -NH₂ groups. The presence and amount of hydroxyl groups on the surface play an important role in photocatalytic reactions. FTIR spectra show how Ga(III) loading affects the number or type of hydroxyl groups. Increasing the number of hydroxyl groups is generally associated with more hydroxyl radical formation and hence higher photocatalytic activity. The peaks at 2870 cm⁻¹ and 1444 cm⁻¹ are thought to belong to asymmetric C-H sp³ and C-H sp² bending vibrations, respectively [36]. However, the N-H bending vibration of chitosan at 1581 cm⁻¹ and PESA's symmetric -SO₃ stretching vibration at 1022 cm⁻¹ are observed [36], [37]. The peak at 1384 cm⁻¹

¹ corresponds to CH₃ symmetric deformation [38]. Another result obtained from the FTIR spectra of the composite material formed by combining different components such as PESA and chitosan is that there is an interaction between these components and that the composite is formed by supporting new bond formations. The distribution and binding type of Ga(III) ions in the polymer/polysaccharide matrix are also clearly shown by the peaks. With the addition of Ga(III), the peak at 2931 cm⁻¹ and 612 cm⁻¹ belongs to Ga-N stretching vibration [39], [40], while the peak at 476 cm⁻¹ belongs to Ga-O stretching vibration [41].

FTIR spectra of PESA/Cht and PESA-Ga(III)/Cht spheres are given in Figure 2.

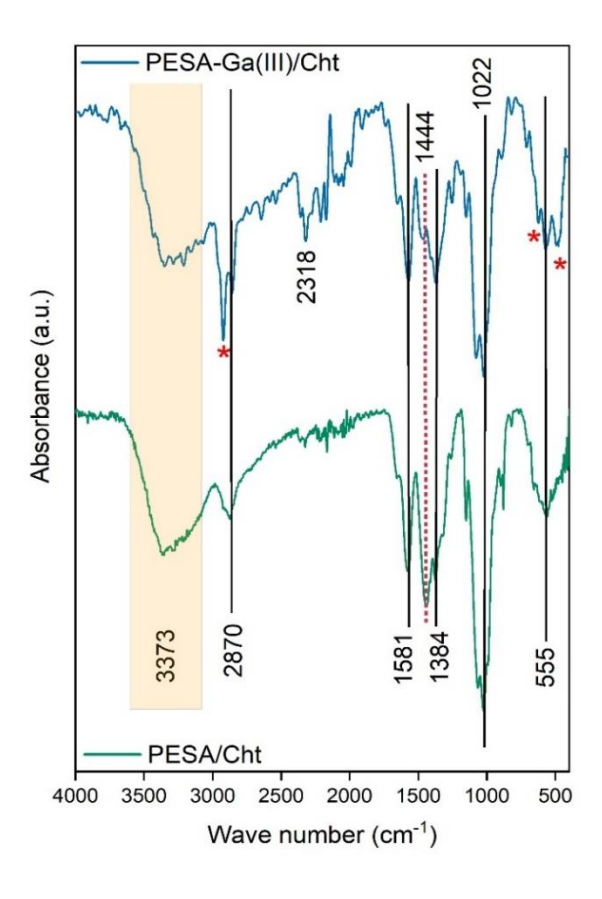


Figure 2. FTIR spectrum of PESA/Cht and PESA-Ga(III)/Cht spheres

The changes in the FTIR spectra due to the loading of Ga(III) ions indicate that the metal ions interact with the polymer/polysaccharide structure without causing a negative effect and as a result, the surface properties are such that they increase the photocatalytic effect. The new active sites formed by the loading of Ga(III) and the changing surface charge led us to comment that they will affect the adsorption of pollutants and the reaction rate. The peaks of new Ga-O or Ga-N bonds in the PESA-Ga(III)/Cht spectrum indicate that these Ga(III) ions are successfully attached to the sphere surface. These new metal centers are interpreted to increase light absorption, facilitate the formation of electron-hole pairs and thus improve photocatalytic

activity. Shifts in vibration frequencies of functional groups in chitosan and/or PESA with Ga(III) loading indicate changes in the electronic structure and chemical properties of the surface. These changes are considered to increase photocatalytic performance by affecting the adsorption and activation of pollutant molecules. The interactions between PESA and chitosan and the integration of Ga(III) ions into this structure may affect the overall photocatalytic performance of the material. These interactions and structural changes after loading were evaluated by FTIR analysis. As a result, the comparison and analysis of the FTIR spectra of PESA/Cht and PESA-Ga(III)/Cht spheres showed the involvement of Ga(III) ions in the chemical structure of the material.

3.3 UV Analysis

Figure 3 shows the UV spectra of PESA/Cht and PESA-Ga(III)/Cht spheres.

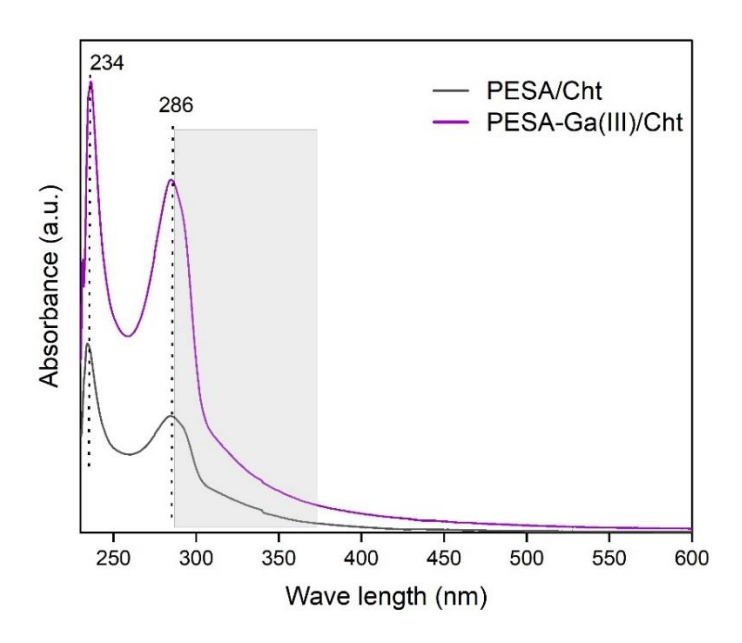


Figure 3. UV-VIS spectra of PESA/Cht and PESA-Ga(III)/Cht spheres

According to the UV spectra of the spheres, a band belonging to chitosan is observed at 286 nm. This band is thought to be due to the n- σ^* transition [42]. At 234 nm, a band of PESA was observed due to the π - π^* transition. Band broadening occurs in the UV spectrum of PESA-Ga(III)/Cht spheres due to the electrostatic interaction of Ga(III).

The band gap of PESA-Ga(III)/Cht spheres was determined using the Tauc's equation.

$$(Ahv)^2 = B(hv - Eg) \tag{2}$$

Here, A is the absorption coefficient, B is the proportionality constant, h is the Planck constant, and v is the frequency [43].

The energy difference between the valence (π) and conduction (π^*) bands determines the band (Eg) that determines the optical property of the material. According to the Tauc's equation, the band gap of PESA-Ga(III)/Cht spheres was determined as 4.14 eV.

3.4 Photocatalytic Effect

The photocatalytic effect of PESA-Ga(III)/Cht spheres on MB dye was determined under UV light. The photocatalytic activity was determined by considering the decrease in the maximum absorption peak of the dye at 664 nm.

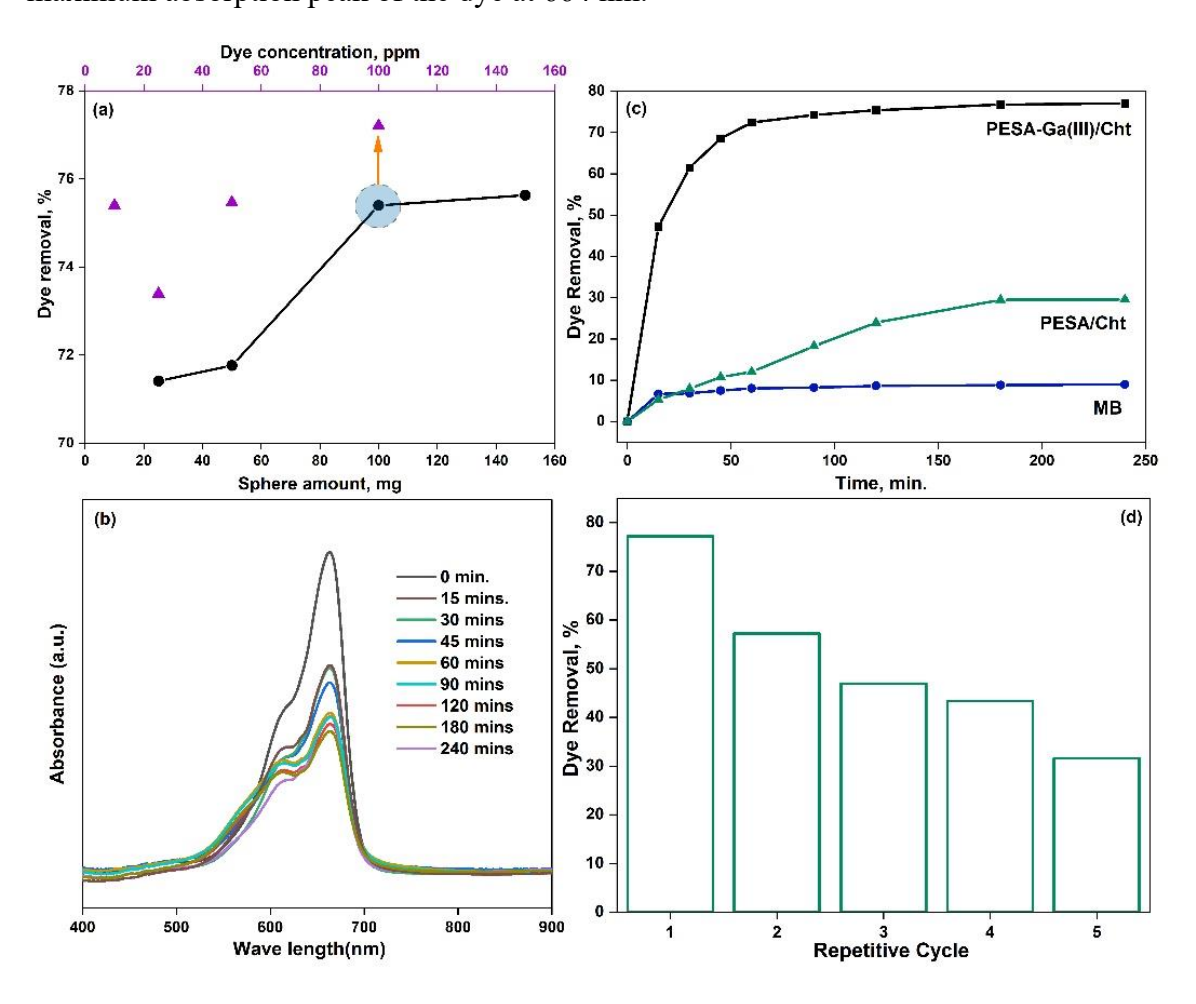


Figure 4. (a) Determination of optimum conditions for the photocatalytic effect of MB, (b) The PESA-Ga(III)/Cht shapes catalyzed photocatalytic degradation of MB over time (Concentration of MB 100 ppm (10 mL), Ga(III)/Cht shapes amount: 100 mg, UV irradiation at 365 nm). (c) The PESA-Ga(III)/Cht, PESA/Cht shapes and without shapes percentage degradation of MB (d) Repetitive tests for photocatalyst PESA-Ga(III)/Cht shapes for five cycle of MB

To determine the photocatalytic effect of PESA-Ga(III)/Cht spheres on MB, firstly sphere amount study (MB of concentration 10 ppm, V=10 mL) was performed (Figure 4a). After stirring with 25, 50, 100, and 150 mg sphere amounts under 365 nm UV light for 2 hours, the photocatalytic effect was determined as 71.41, 71.76, 75.39 and 75.62%, respectively.

After determining that a 100 mg sphere was suitable for the photocatalytic effect, the photocatalytic effect on dye concentration was investigated. The photocatalytic effect at 10, 25, 50, and 100 ppm dye concentration under the same conditions (sphere amount 100 mg, dye solution volume 10 mL) was determined as 75.39, 73.39, 75.46, and 77.20 %, respectively.

The degradation of the dye over time in the presence of PESA-Ga(III)/Cht catalyst is shown in Figure 4b. After the first 60 minutes, it was observed that the photocatalytic effect did not increase significantly, and the degradation rate of the dye decreased. The degradation of the dye of PESA-Ga(III)/Cht, PESA/Cht shapes and without shapes is show in Figure 4c. The PESA-Ga(III)/Cht catalyst, 77.20% of the dye is degraded after 240 minutes, while this rate decreases to 29.55% in the presence of PESA/Cht catalyst. It is thought that Ga(III) supplementation enhances the photocatalytic degradation. Additionally, the photocatalytic degradation of the dye without a catalyst was determined to be 9.01%. Accordingly, it is seen that the photocatalytic degradation of the dye is quite limited without a catalyst.

Figure 4d shows the five repeated uses of the photocatalyst under the same conditions. Accordingly, the photocatalytic effect decreased from the first to the fifth use (77.2%, 57.2%, 46.93%, 43.35%, and 31.58%), respectively. This decrease is likely due to the dye blocking the active sites on the photocatalyst surface.

Kinetic modeling was performed using pseudo-first-order equations using Equation (3) and pseudo-second-order equations using Equation (4) [44].

$$ln\frac{C_t}{C_o} = -k.t (3)$$

$$\frac{1}{C_t} - \frac{1}{C_0} = k.t \tag{4}$$

Here, C_o is the initial concentration, C_t is the concentration at t, k is the rate constant, and t is the time.

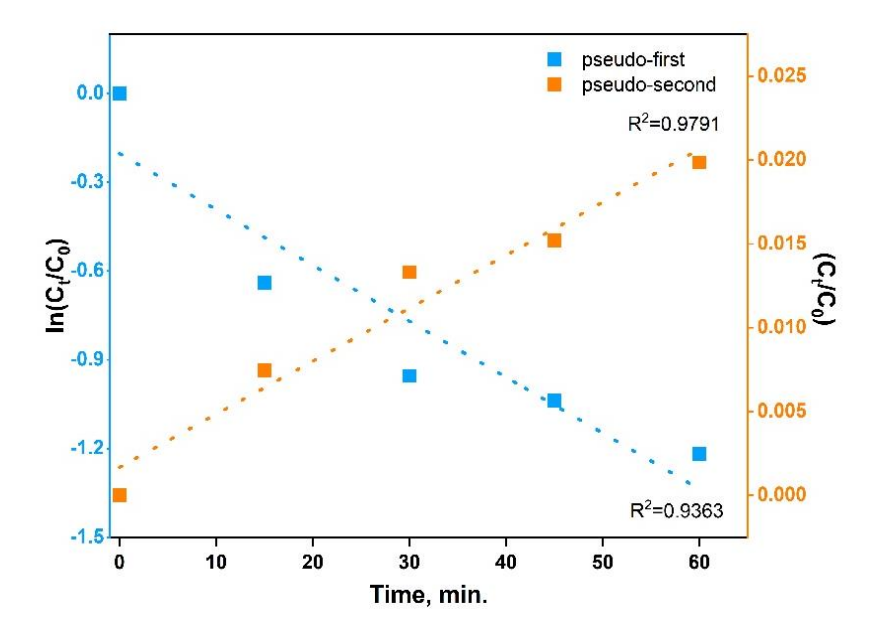


Figure 5. Kinetics for the MB decomposition

Figure 5 shows that the graph drawn according to the pseudo-second-order kinetic model is more linear than the pseudo-first-order kinetic model. The degradation is more suitable for the pseudo-second-order kinetic model, where the rate constant k is determined as 0.0003 min⁻¹ (R^2 =0.9791). Accordingly, the degradation is likely due to photochemical degradation and the interaction of the dye with the active sites on the surface of the photocatalyst.

4 CONCLUSION AND SUGGESTIONS

This study investigated the photocatalytic effect of PESA-Ga(III)/Cht spheres on methylene blue, a cationic dye. FTIR, UV-VIS, SEM, and ICP-OES analysis characterized the synthesized PESA-Ga(III)/Cht spheres. FTIR and UV-VIS spectra confirmed the functional groups in the polymer structures and their interaction with Ga(III). SEM micrographs showed a homogeneous, spherical morphology with an average size of 1.014±0.03 mm. Finally, the photocatalytic activity of PESA-Ga(III)/Cht spheres was evaluated for the degradation of MB under UV light and showed 77.2% photocatalytic activity. As a result, a promising, low-cost, and efficient photocatalyst for environmental applications was proposed.

Statement of Research and Publication Ethics

The study is complied with research and publication ethics.

Artificial Intelligence (AI) Contribution Statement

This manuscript was entirely written, edited, analyzed, and prepared without the assistance of any artificial intelligence (AI) tools. All content, including text, data analysis, and figures, was solely generated by the authors.

REFERENCES

- [1] R. Sivakumar and N. Y. Lee, "Adsorptive removal of organic pollutant methylene blue using polysaccharide-based composite hydrogels," *Chemosphere*, vol. 286, Jan. 2022, doi: 10.1016/j.chemosphere.2021.131890.
- [2] M. Gavrilescu, K. Demnerová, J. Aamand, S. Agathos, and F. Fava, "Emerging pollutants in the environment: Present and future challenges in biomonitoring, ecological risks and bioremediation," *N Biotechnol*, vol. 32, no. 1, pp. 147–156, Jan. 2015, doi: 10.1016/j.nbt.2014.01.001.
- [3] N. Wang, J. Chen, J. Wang, J. Feng, and W. Yan, "Removal of methylene blue by Polyaniline/TiO₂ hydrate: Adsorption kinetic, isotherm and mechanism studies," *Powder Technol*, vol. 347, pp. 93–102, Apr. 2019, doi: 10.1016/j.powtec.2019.02.049.
- [4] F. Mashkoor and A. Nasar, "Magsorbents: Potential candidates in wastewater treatment technology A review on the removal of methylene blue dye," Apr. 15, 2020, *Elsevier B.V.* doi: 10.1016/j.jmmm.2020.166408.
- [5] H. N. Hamad and S. Idrus, "Recent Developments in the Application of Bio-Waste-Derived Adsorbents for the Removal of Methylene Blue from Wastewater: A Review," Feb. 01, 2022, MDPI. doi: 10.3390/polym14040783.
- [6] S. E. Abo-Neima, M. M. El-Sheekh, M. I. Al-Zaban, and A. I. M. EL-Sayed, "Antibacterial and anticorona virus (229E) activity of Nigella sativa oil combined with photodynamic therapy based on methylene blue in wound infection: in vitro and in vivo study," *BMC Microbiol*, vol. 23, no. 1, Dec. 2023, doi: 10.1186/s12866-023-03018-1.
- [7] K. Evren *et al.*, "A case of peritonitis caused by Wickerhamomyces anomalus (Candida pelliculosa) related to peritoneal dialysis," *Mikrobiyol Bul*, vol. 55, no. 4, pp. 665–672, 2021, doi: 10.5578/mb.20219718.
- [8] A. Krishna Moorthy, B. Govindarajan Rathi, S. P. Shukla, K. Kumar, and V. Shree Bharti, "Acute toxicity of textile dye Methylene blue on growth and metabolism of selected freshwater microalgae," *Environ Toxicol Pharmacol*, vol. 82, Feb. 2021, doi: 10.1016/j.etap.2020.103552.
- [9] J. Jiang *et al.*, "Rapid photodegradation of methylene blue by laser-induced plasma," *RSC Adv*, vol. 12, no. 33, pp. 21056–21065, Jul. 2022, doi: 10.1039/d2ra03633a.
- [10] D. Doğan, R. Taş, and M. Can, "Increasing Photocatalytic Stability and Photocatalytic Property of Polyaniline Conductive Polymer," *Iran J Sci Technol Trans A Sci*, vol. 44, no. 4, pp. 1025–1037, Aug. 2020, doi: 10.1007/s40995-020-00922-3.
- [11] H. Bai *et al.*, "Synergistic effects of rare-metal ytterbium doping on TiO₂/g-C₃N₅ heterostructures for enhanced photocatalytic degradation of methylene blue," *Inorg Chem Commun*, vol. 175, May 2025, doi: 10.1016/j.inoche.2025.114159.
- [12] A. Chawla *et al.*, "Recent advances in synthesis methods and surface structure manipulating strategies of copper selenide (CuSe) nanoparticles for photocatalytic environmental and energy applications," Aug. 01, 2024, *Elsevier Ltd.* doi: 10.1016/j.jece.2024.113125.
- [13] S. Sharma *et al.*, "Critical review on the tetracycline degradation using photo-Fenton assisted g-C₃N₄-based photocatalysts: Modification strategies, reaction parameters, and degradation pathway," *J Environ Chem Eng*, vol. 12, no. 3, Jun. 2024, doi: 10.1016/j.jece.2024.112984.
- [14] Z. Demirkaya et al., "Purification of Textile Dye by Photocatalytic Oxidation Process Using Metal Modified Chitosan Balls," *Journal Of Şura Akademi*, vol 8, 2025.

- [15] A. Nithya, K. Jothivenkatachalam, S. Prabhu, and K. Jeganathan, "Chitosan based nanocomposite materials as photocatalyst a review," *Materials Science Forum*, vol. 781, pp. 79–94, 2014, doi: 10.4028/www.scientific.net/MSF.781.79.
- [16] A. Buasri, K. Rochanakit, W. Wongvitvichot, U. Masa-Ard, and V. Loryuenyong, "The Application of Calcium Oxide and Magnesium Oxide from Natural Dolomitic Rock for Biodiesel Synthesis," in *Energy Procedia*, Elsevier Ltd, Nov. 2015, pp. 562–566. doi: 10.1016/j.egypro.2015.11.534.
- P. Swarnakar *et al.*, "Silver deposited titanium dioxide thin film for photocatalysis of organic compounds using natural light," *Solar Energy*, vol. 88, pp. 242–249, Feb. 2013, doi: 10.1016/j.solener.2012.10.014.
- [18] M. Alharbi, M. waqas Iqbal, Y. Al-Hadeethi, and M. A. Hussein, "Photocatalytic activity of composite material-based nylon 6/sulfur NPs and reinforced carbon nanotubes," *Diam Relat Mater*, vol. 151, Jan. 2025, doi: 10.1016/j.diamond.2024.111859.
- [19] R. L. Pereira Rocha *et al.*, "Gallium-containing hydroxyapatite as a promising material for photocatalytic performance," *Minerals*, vol. 11, no. 12, Dec. 2021, doi: 10.3390/min11121347.
- [20] K. Pajor, Ł. Pajchel, A. Zgadzaj, U. Piotrowska, and J. Kolmas, "Modifications of hydroxyapatite by gallium and silver ions—physicochemical characterization, cytotoxicity and antibacterial evaluation," *Int J Mol Sci*, vol. 21, no. 14, pp. 1–15, Jul. 2020, doi: 10.3390/ijms21145006.
- [21] V. S. Kujur and S. Singh, "Structural, magnetic, optical and photocatalytic properties of GaFeO₃ nanoparticles synthesized via non-aqueous solvent-based sol-gel route," *Journal of Materials Science: Materials in Electronics*, vol. 31, no. 20, pp. 17633–17646, Oct. 2020, doi: 10.1007/s10854-020-04318-2
- [22] R. Messemeche, Y. Benkhetta, A. Attaf, H. Saidi, M. S. Aida, and O. Ben khetta, "Photocatalytic mechanisms reactions of gallium doped TiO₂ thin films synthesized by sol gel (spin coating) in the degradation of methylene blue (MB) dye under sunlight irradiation," *Reaction Kinetics, Mechanisms and Catalysis*, vol. 135, no. 5, pp. 2735–2747, Oct. 2022, doi: 10.1007/s11144-022-02288-6.
- [23] K. Parveen, U. Rafique, I. Jamil, and A. Ashraf, "Photodegradation of Rhodamine B using gallium hybrids as an efficient photocatalyst," *Environ Monit Assess*, vol. 195, no. 9, Sep. 2023, doi: 10.1007/s10661-023-11683-y.
- [24] A. A. Nayl *et al.*, "A novel method for highly effective removal and determination of binary cationic dyes in aqueous media using a cotton-graphene oxide composite," *RSC Adv*, vol. 10, no. 13, pp. 7791–7802, Feb. 2020, doi: 10.1039/c9ra09872k.
- [25] B. Soman, S. Challagulla, S. Payra, S. Dinda, and S. Roy, "Surface morphology and active sites of TiO₂ for photoassisted catalysis," *Research on Chemical Intermediates*, vol. 44, no. 4, pp. 2261–2273, Apr. 2018, doi: 10.1007/s11164-017-3227-6.
- [26] R. K. Arya *et al.*, "Polymer Coated Functional Catalysts for Industrial Applications," May 01, 2023, *MDPI*. doi: 10.3390/polym15092009.
- [27] J. M. Blasi, P. J. Weddle, C. Karakaya, D. R. Diercks, and R. J. Kee, "Modeling reaction-diffusion processes within catalyst washcoats: II. Macroscale processes informed by microscale simulations," 2016.
- [28] W. Xie *et al.*, "Polydopamine Shell as a Ga3+ Reservoir for Triggering Gallium–Indium Phase Separation in Eutectic Gallium–Indium Nanoalloys," *ACS Nano*, vol. 15, no. 10, pp. 16839–16850, Oct. 2021, doi: 10.1021/acsnano.1c07278.
- [29] M. N. Cardoza-Contreras, A. Vásquez-Gallegos, A. Vidal-Limon, J. M. Romo-Herrera, S. Águila, and O. E. Contreras, "Photocatalytic and antimicrobial properties of Ga doped and Ag doped ZnO nanorods for water treatment," *Catalysts*, vol. 9, no. 2, Feb. 2019, doi: 10.3390/catal9020165.
- [30] Y. Xu, The photoelectronic properties of chalcogenide glass ceramic. *Material chemistry. Université de Rennes*, 2014.
- [31] L. L. Zhou, G. Wu, J. Liu, and X. Bin Yu, "Preparation of Ga³⁺:ZnO quantum dots and the photoelectric properties of sensitized polycrystalline silicon solar cells," *Chemical Papers*, vol. 75, no. 2, pp. 805–811, Feb. 2021, doi: 10.1007/s11696-020-01339-3.
- [32] M. Faqrul and A. Chowdhury, "Unassisted Photocatalytic Overall Pure Water Splitting Using III-Nitride Nanostructures," 2018.

- [33] M. S. Akhtar, A. Umar, S. Sood, I. S. Jung, H. H. Hegazy, and H. Algarni, "Rapid growth of TiO₂ nanoflowers via low-temperature solution process: Photovoltaic and sensing applications," *Materials*, vol. 12, no. 4, Feb. 2019, doi: 10.3390/ma12040566.
- [34] S. Buapoon, A. Phuruangrat, P. Dumrongrojthanath, T. Thongtem, and S. Thongtem, "Sonochemical Synthesis and Characterization of Ag/ZnO Heterostructure Nanocomposites and their Photocatalytic Efficiencies," *J Electron Mater*, vol. 50, no. 8, pp. 4524–4532, Aug. 2021, doi: 10.1007/s11664-021-08985-7.
- [35] Y. Wang, Y. Feng, J. Jiang, and J. Yao, "Designing of Recyclable Attapulgite for Wastewater Treatments: A Review," *ACS Sustain Chem Eng*, vol. 7, no. 2, pp. 1855–1869, Jan. 2019, doi: 10.1021/acssuschemeng.8b05823.
- [36] M. Nora, A. Bhagaskara, V. Agustisari, A. Lim, H. R. Alfalah, and D. Siswanta, "Fabrication of Polystyrene Sulfonate-Chitosan (PSS-Chitosan) Membrane as Dodecyl Benzene Sulfonate (DBS) Adsorbent in Laundry Wastewater," *Jurnal Kimia Sains dan Aplikasi*, vol. 26, no. 1, pp. 19–27, Jan. 2023, doi: 10.14710/jksa.26.1.19-27.
- Ž. Petrović, M. Ristić, and S. Musić, "The effect of sodium polyanethol sulfonate on the precipitation of zinc oxide," *J Alloys Compd*, vol. 694, pp. 1331–1337, 2017, doi: 10.1016/j.jallcom.2016.10.111.
- [38] M. F. Queiroz, K. R. T. Melo, D. A. Sabry, G. L. Sassaki, and H. A. O. Rocha, "Does the use of chitosan contribute to oxalate kidney stone formation?," *Mar Drugs*, vol. 13, no. 1, pp. 141–158, Jan. 2015, doi: 10.3390/md13010141.
- [39] O. Adewuyi, A. B. Alabi, F. H. Abejide, and F. O. Omoniyi, "Impact of Nitridation on the Structural, Optical, and Morphological Properties of Solvothermally Synthesized Gallium Nitride Nanoparticles," Mar. 11, 2025. doi: 10.21203/rs.3.rs-6145110/v1.
- [40] A. K. Mallik, G. Krishnamurthy, W.-C. Shih, P. Pobedinskas, J. D'Haen, and K. Haenen, "Enhanced etching of GaN with N₂ gas addition during CVD diamond growth," *Functional Diamond*, vol. 4, no. 1, Dec. 2024, doi: 10.1080/26941112.2024.2393817.
- [41] H. J. Bae *et al.*, "High-aspect ratio β-Ga₂O₃ nanorods via hydrothermal synthesis," *Nanomaterials*, vol. 8, no. 8, Aug. 2018, doi: 10.3390/nano8080594.
- [42] Q. Ruan et al., "Development of ZnO/selenium nanoparticles embedded chitosan-based anti-bacterial wound dressing for potential healing ability and nursing care after peadiatric fracture surgery," *Int Wound J.*, vol 20, no. 6 pp. 1819-1831. doi: 10.1111/iwj.13947.
- [43] A. Şenocak, H. Akbaş, and B. İşgör, "NiO Nanoparticles Via Calcination of Dithiocarbamate Pioneers: Characterization and Photocatalytic Activity," *Bitlis Eren Üniversitesi Fen Bilimleri Dergisi*, vol. 13, no. 4, pp. 969–978, Dec. 2024, doi: 10.17798/bitlisfen.1485060.
- [44] N. N. Bahrudin, "Evaluation of degradation kinetic and photostability of immobilized TiO₂/activated carbon bilayer photocatalyst for phenol removal," *Applied Surface Science Advances*, vol. 7, Feb. 2022, doi: 10.1016/j.apsadv.2021.100208.